(AIAA 99-3177, AIAA 17th Applied Aerodynamics Conference, Norfolk, VA, June 1999)

COMPUTATIONAL MODELING FOR THE FLOW OVER A MULTI-ELEMENT AIRFOIL

William W. Liou* and Fengjun Liu**
Department of Mechanical and Aeronautical Engineering
Western Michigan University
Kalamazoo, MI 49008

Abstract

The flow over a multi-element airfoil is computed using two two-equation turbulence models. The computations are performed using the INS2D Navier-Stokes code for two angles of attack. Overset grids are used for the three-element airfoil. The computed results are compared with experimental data for the surface pressure, skin friction coefficient, and velocity magnitude. The computed surface quantities generally agree well with the measurement. The computed results reveal the possible existence of a mixing-layer-like region of flow next to the suction surface of the slat for both angles of attack.

I. Introduction

Flows past multi-element airfoils have been subjected to intensive experimental and computational studies[1,2,3] for the past two decades. An accurate prediction of such flows can enhance the performance and the safety factor of aircrafts in high-lift operations. Even with the advances of computational fluid dynamics (CFD), the prediction of high-lift flow fields remains a challenge. The flow fields around multi-element airfoils are complex and are known to be dominated by different flow mechanisms at different operating conditions.

A significant portion of the flow around multi-element airfoils is transitional over a wide range of operating condition. The onset location of the transition process varies with, for example, angles of attack and Reynolds numbers. In addition to boundary layer transition, free shear flow transition is also likely to occur in, for example, the flow over the slat.

As the slat wake convects downstream, it may further interact with the transitional flow over the succeeding elements, such as the flow over the main element and the flap. As a result, an accurate prediction of the flow transition represents a major challenge for the computation of the flow over multi-element airfoils and the use of a transition model often becomes a discriminating factor in the outcomes of a prediction. Turbulence models are frequently used in the high-lift flow calculations. In this practice, turbulence models are "turned-on" at a designated location on the airfoils. The designated locations are usually correlated with the measured location of transition onset and the computational results can vary significantly with the assigned transition location.

In this paper, the flow fields over a multi-element airfoil are calculated numerically using two two-equation turbulence models.

These computational exercises are necessary in an effort to identify the limitation of turbulence models in the prediction of transitional flows. The computational results may also help to investigate areas of the flow where experimental data are difficult to obtain.

The Navier-Stokes solver used in the study is described in the next section. The Chimera composite grids used are also presented.

II. Flow Solver

The flow calculations presented here were performed with the INS2D code[4,5,6]. The code solves the two-dimensional, incompressible form of the Reynolds-averaged Navier-Stokes equations using an artificial compressibility approach. The INS2D code is a finite difference solver, using Roe's third order upwind-biased, flux-difference splitting for the convective terms and a second-order central differencing for the viscous terms. The code is capable of solving both steady and unsteady problems with point-to-point matched grids or Chimera overset grids. The details of the INS2D code can be found in the references cited above. The

---

* Associate Professor, Senior Member AIAA.

**Graduate Student.

INS2D code has been applied extensively to the flow over various single- and multi-element airfoils[4,5,6] and has been shown to be a very reliable tool for such purposes. Generating the necessary grids for multi-element airfoil flow calculations can be very time-consuming regardless of the grid topology one chooses to use. In this study, overset grids were used and the grids were generated using the OVERMAGG[7] software. OVERMAGG is an automated script system specifically designed to perform overset grid generation for multi-element airfoils. The use of OVERMAGG has resulted in a significant amount of saving in time during this study.

III. Turbulence Models

The SST model[8] and a $k-\varepsilon$[9,10,11] model were used to study the flow field. The SST model is available as a model option in the INS2D code. The $k-\varepsilon$ model was recently implemented as a separate module to the code. There are two other one-equation model options in the INS2D code. The SST and the two one-equation models have been applied to the flow over the 30P30N geometry and the results have been reported previously[3].

The SST model was designed to take advantange of both the robustness of the $k-\omega$ type of models in the near wall region and the free-stream independence of the $k-\varepsilon$ type of models in the outer part of boundary layers and for free shear layers. The eddy-viscosity was formulated to account for the transport of the principal turbulent shear stress in boundary layers. The SST model has been shown to perform very well for many different flows.

The $k-\varepsilon$ model used here represents a variant of the model developed by Shih and Lumley[9], with the constant $C_\mu(=0.09)$ replaced by a variable C_μ formulation. The new formulation of C_μ, with an explicit dependence on the mean strain rate, was developed based on the realizability constraints of the Reynolds stresses. The model has been shown to work well for a wide range of flows[10,11].

The model equations for k and ϵ are,

$$k_{,t} + U_i k_{,i} = [(\nu + \nu_t)k_{,i}]_{,i} - \overline{u_i u_j} U_{i,j} - \varepsilon \qquad (1)$$

$$\varepsilon_{,t} + U_i \varepsilon_{,i} = [(\nu + \frac{\nu_t}{\sigma_\varepsilon})\varepsilon_{,i}]_{,i} - C_1 \frac{\varepsilon}{k} \overline{u_i u_j} U_{i,j} - C_2 f_2 \frac{\varepsilon^2}{k} + \nu \nu_t S_{,i} S_{,i} \qquad (2)$$

where

$$C_1 = 1.44, \quad C_2 = 1.92, \quad \sigma_\varepsilon = 1.3$$

$$f_2 = 1 - 0.22\exp[-(\frac{R_t}{6})^2], \quad R_t = \frac{k^2}{\nu\varepsilon}$$

$$C_\mu = \frac{1}{A_0 + A_s U^{(*)} \frac{k}{\varepsilon}} \qquad (3)$$

where

$$U^{(*)} = \sqrt{S_{ij}S_{ij} + \tilde{\Omega}_{ij}\tilde{\Omega}_{ij}}$$

$$\tilde{\Omega}_{ij} = \tilde{\Omega}_{ij} - 2\epsilon_{ijk}\omega_k$$

$$\tilde{\Omega}_{ij} = \Omega_{ij} - \epsilon_{ijk}\omega_k$$

Ω_{ij} is the mean rotation rate viewed in a rotating reference frame with the angular velocity ω_k. The parameter A_s is determined by

$$A_s = \sqrt{6}\cos\phi, \quad \phi = \frac{1}{3} arc\cos(\sqrt{6}W)$$

$$W = \frac{S_{ij}S_{jk}S_{ki}}{\tilde{S}^3} \qquad (4)$$

$$\tilde{S} = \sqrt{S_{ij}S_{ij}}, \quad S = \sqrt{2S_{ij}S_{ij}}$$

The damping function is defined by

$$f_\mu = [1. - \exp(-(a_1 R_k + a_3 R_k^3 + a_5 R_k^5))]^{\frac{1}{2}} \qquad (5)$$

where

$$a_1 = 1.7 \times 10^{-3}, \quad a_3 = 10^{-9}, \quad a_5 = 5 \times 10^{-10}$$

$$R_k = \frac{\sqrt{k}y}{\nu}$$

The near-wall boundary conditions for the turbulent quantities are

$$k = 0.25u_\tau^2 \quad \text{and} \quad \varepsilon = 0.251\frac{u_\tau^4}{\nu} \qquad (6)$$

where u_τ denotes the surface friction velocity.

IV. Geometry

The McDonnell Douglas 30P-30N landing configuration was used in this study. Figure 1 shows the geometry and the stations where profile data will be presented. Both the leading-edge slat and the trailing-edge flap have a deflection angle of 30°. The airfoil has been tested extensively at NASA Langley Low-Turbulence Pressure Tunnel (LTPT)[1,12]. The geometry has been used as a test case in a *CFD Challenge Workshop* held at NASA Langley in 1993 and many computational results obtained by using different solvers and models have been reported[2,3,6].

The computational grid consists of seven zones and a total of about 103,000 grid points. Figure 2 shows the C grids around the slat, the main element, and the

flap, which consist of 175×45, 381× 133, and 221×85 points, respectively. Two H grids were used for the main-element cove and for the wake region of the flap. A background H grid extends to the top and the bottom walls of the wind tunnel. When the grid for one element overlaps another element(s), holes and outer boundaries are determined by using the PEGSUS code. The communicaiton between the overset grids are also handled by the PEGSUS code.

Comprehensive grid-independence studies have been performed and reported previously using similar overset grids for the same geometry[3,6]. These and other calculations for the same geometry indicate that the grid point distributions in the wake regions can have certain effects on the velocity profiles in those regions and the wall pressure is not sensitive to the grid density. These results also show that further refinement of the grid from the current level does not change the results appreciably.

It should be noted that the turbulence models were applied without including any explicit account for the flow transition.

Results will be presented for a Reynolds number of nine million and two angles of attack (AOA) of 8° and 19°.

V. Results and Discussions

Figure 3 shows the comparison of the surface pressure coefficient distributions for the 19° case. Both models predict the surface pressure well with a slightly faster external flow predicted by the $k-\varepsilon$ model over the suction surface of the slat.

For AOA=8^0, the surface pressure coefficient distributions are shown in Figure 4. The overall agreement with the measurement is good for the main element and the flap. On the suction surface of the slat, the $k-\varepsilon$ model is predicting a faster external flow.

Figure 5 shows the velocity profiles on the main element and on the flap for AOA=19^0. At $x/c = 0.1075$, there is almost an uniform offset between the data and the predictions. This may have been caused by possible improper data calibration[2]. The predicted slat wake is located slightly further away from the main element surface at all three stations (x/c=0.1075, 0.45, and 0.85). As a result, the merging of the slat wake and the boundary layer is apparently yet to occur at $x/c = 0.85$. The boundary layer velocity profiles were predicted well by the $k-\varepsilon$ model, which resulted in a better prediction of the main wake immediatedly behind the main element trailing edge (Figure 5.d, $x/c = 0.89817$).

On the flap (Figures 5.e and 5.f, $x/c = 1.0321$ and 1.1125), there seems to be a better overall agreement between the $k-\varepsilon$ model and the measurement in terms of the development of the slat and the main-element wakes. None of the models gives a good prediction for the deficit of the main-element wake.

Figure 6 shows the velocity profiles on the main element for AOA=8^0. The slat wake is predicted well at $x/c = 0.1075$. The predicted main element surface boundary layer is more developed than what the data has shown. At the later stations, $x/c = 0.45$ and 0.85, the predicted velocity profiles agree well the measurement.

Figure 7 shows the surface skin friction coefficient distributions on the main element for AOA=19°. The computed results agree very well with the available measured data.

It should be noted that correction terms for transition modeling have been proposed for both models[2,3,13]. These corrections have not been included in the calculations presented here.

It is apparent that, based on the results shown here and those published in the previous studies, the two turbulence models used in this study can give a fairly accurate account of the outer inviscid flow field around the multi-element airfoil. The near wall viscous flow regions have not been predicted well. A measure commonly adpoted to improve the prediction of the near wall viscous flow was to include some type of correction terms for the boundary layer transition, as the measurement did show a fairly large region of boundary layer transition on all three elements for a range of flow conditions. Various approaches have been proposed[2,3] and have shown a significant improvement. These results indicate that the slat flow prediciton plays a critical role in the overall flow computation.

The flow field around the slat is complicated and difficult to measure due to the small sizes of the slat. The laminar/turbulent separation and reattchment in the lower pressure surface and the boundary layer transition on the upper suction surface have been proposed as among the phenomena that need to be modeled correctly to obtain reasonable predictions. Indeed, Rumsey et al.[2] have shown that the velocity on the main element can be predicted well if the calculated slat wake agrees with the measured wake to begin with.

Since the Reynolds number is large, the initial slat wake development depends largely upon the boundary layer at the point of separation.

In the following, we examine the boundary layer on the suction side of the slat by using the $k-\varepsilon$ model results, hopeing to gain a better understanding of the possible physical mechanisms at play in the slat flow.

Figures 8 and 9 show the distributions of the velocity mangitude and the turbulent kinetic energy profiles in the direction normal to the surface at three locations on the suction side of the slat for AOA=8^0 and 19^0. Note that the velocity magnitude and the turbulent kinetic energy have been normalized by the local skin friction velocity. As the boundary layer on the slat surface develops, it interacts with the outer "inviscid" flow. For AOA=19^0, Figure 8.b shows that, as a result of this interaction, or mixing, of the low speed flow near the surface and the high speed flow in the outer stream, a region of flow with inflectional velocity distribution appears. This mixing phenomana may be similar to that in the free shear layer. The mixing region is also detectible for AOA=8^0 in Figure 8.a, but becomes more apparent further downstream on the slat.

Figure 9 shows that these inflectional velocity distributions have produced local peaks of turbulent kinetic energy in the "mixing" zone of the flow (x/c=-0.071 and 0.0053). For AOA=8^0, the local peaks seem to be developing and, for AOA=19^0, their values have exceeded those in the buffer layer. Therefore, the viscous layer on the slat suction surface exhibits a double-deck structure, with a boundary layer near the wall and mixing-layer-like behavior in the outer region.

As was mentioned earlier, there is no detailed flow profile measurement available for the slat region. The observation made here has been based entirely upon the computed results. However, to the extend that the observation is valid, it is evident that the transition in the shear layer and in the boundary layer are among the essential features of the flow around the slat.

Acknowledgment

This work has been supported by NASA Langley Research Center under a grant NAG 1-1979. The technical monitor is Dr. Ronald D. Joslin. The authors would like to thank Dr. Stuart E. Rogers at NASA Ames Research Center for assistance and advices in using the INS2D and OVERMAGG codes. Dr. Christopher L. Rumsey at NASA Langley Research Center kindly provides the experimental data.

References

[1] A. Bertelrud, "Transition on a three-element high lift configuration at high Reynolds numbers," AIAA paper 98-0703.

[2] C.L. Rumsey, T.B. Gatski, S.X. Ying, and A. Bertelrud, "Prediction of high-lift flows using turbulent closure models," AIAA paper 97-2260.

[3] S.E. Rogers, F.R. Menter, P.A. Durbin, N.N. Mansour, "A comparison of turbulence models in computing multi-element airfoil flows," AIAA paper 94-0291.

[4] S.E. Rogers and D. Kwak, "An upwind differencing scheme for the steady-state incompressible Navier-Stokes equation", *Journal of Applied Numerical Mathematics*, **8**, 43-64, (1991).

[5] S.E. Rogers, S.E., D. Kwak, and C. Kiris, "Numerical solution of the incompressible Navier-Stokes equations for steady-state and time-dependent problems," *AIAA Journal*, **29**, 603-610 (1991).

[6] S.E. Rogers, "A comparison of implicit schemes for the incompressible Navier-Sotkes equations with artificial compressibility," AIAA paper 95-0567.

[7] S.E. Rogers, H.V. Cao, and T.Y. Su, "Grid generation for complex high-lift configurations," AIAA paper 98-3011.

[8] F.R. Menter, "Zonal two equation k-ω turbulence models for aerodynamic flows," AIAA paper 93-2906.

[9] T.-H. Shih and J.L. Lumley, "Kolmogorov behavior of near-wall turbulence and its application in turbulence modeling," *Comp. Fluid Dyn.*, **1**, 43-56 (1993).

[10] W.W. Liou and T.-H. Shih, "Transonic turbulent flow predictions with new two-equation turbulence models", AIAA paper 95-1805.

[11] Z. Yang, N. Georgiadis, J. Zhu, and T.-H. Shih, "Calculations of inlet/nozzle flows using a new $k-\varepsilon$ model," AIAA paper 95-2761.

[12] P.C. Stainback, R.J. McGhee, W.D. Beasley, and H.L. Jr. Morgan, "The Langley Research Center's Low Turbulence Pressure Tunnel," AIAA paper 86-0762.

[13] W.W.Liou and T.-H. Shih, "Bypass transitional flow calculations using a Navier-Stokes solver and two-equation models," AIAA paper 97-2738.

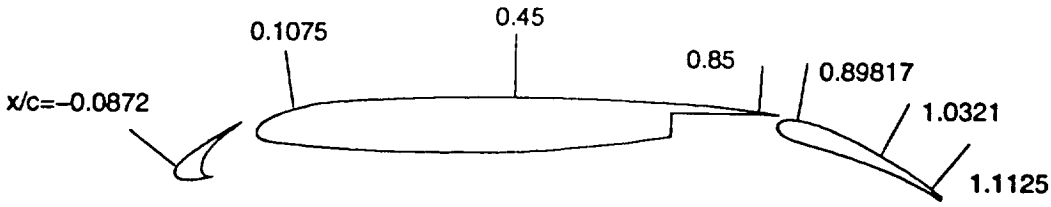

Figure 1. 30P30N geometry and survey stations.

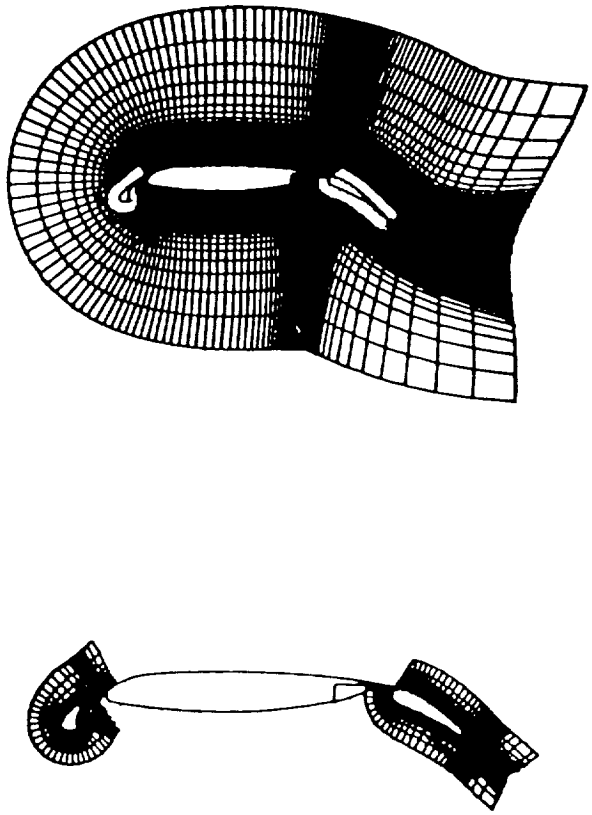

Figure 2. Computational grids

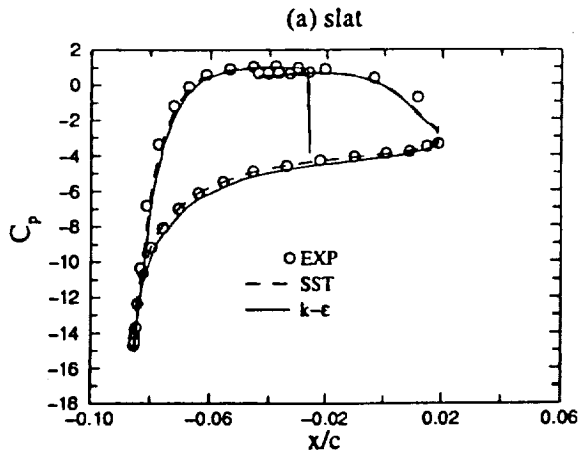

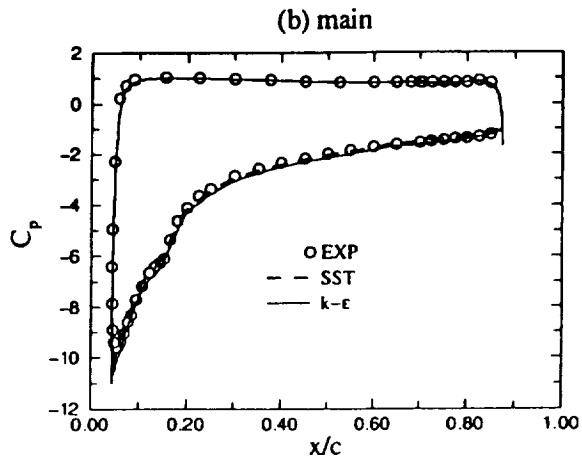

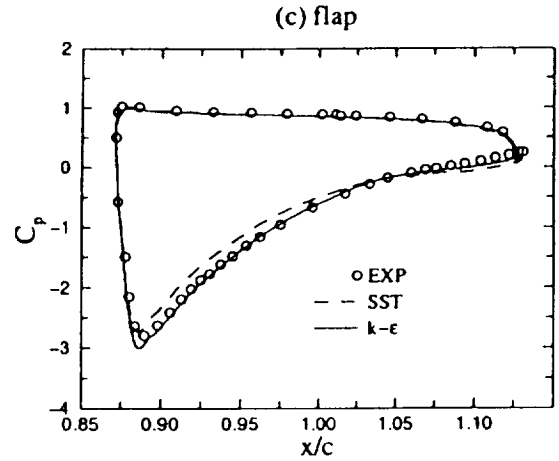

Figure 3. Wall pressure coefficient. 19^0

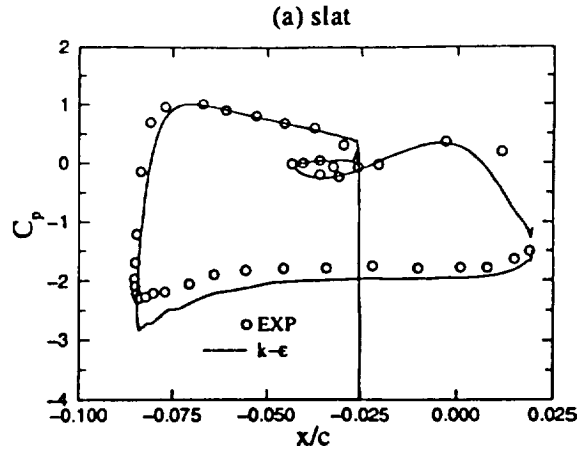

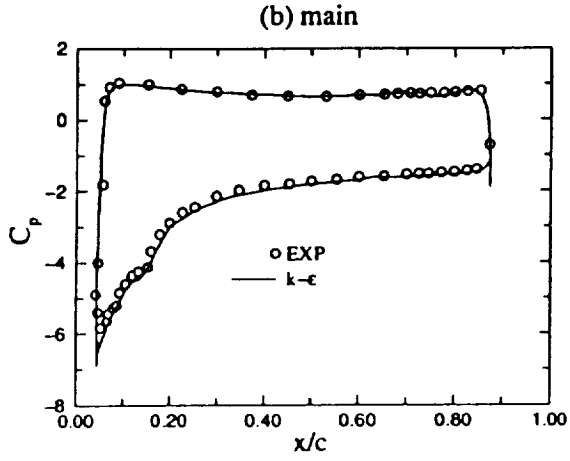

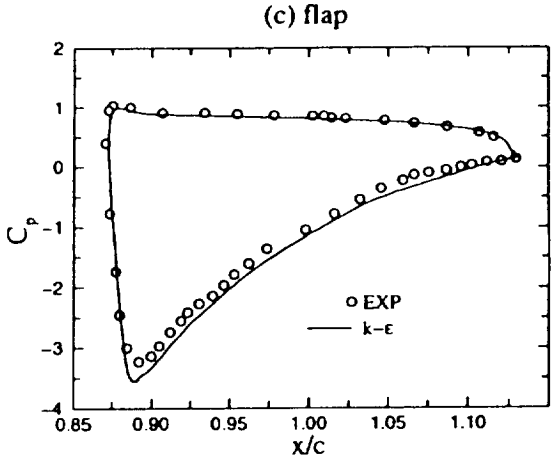

Figure 4. Wall pressure coefficient. 8^0

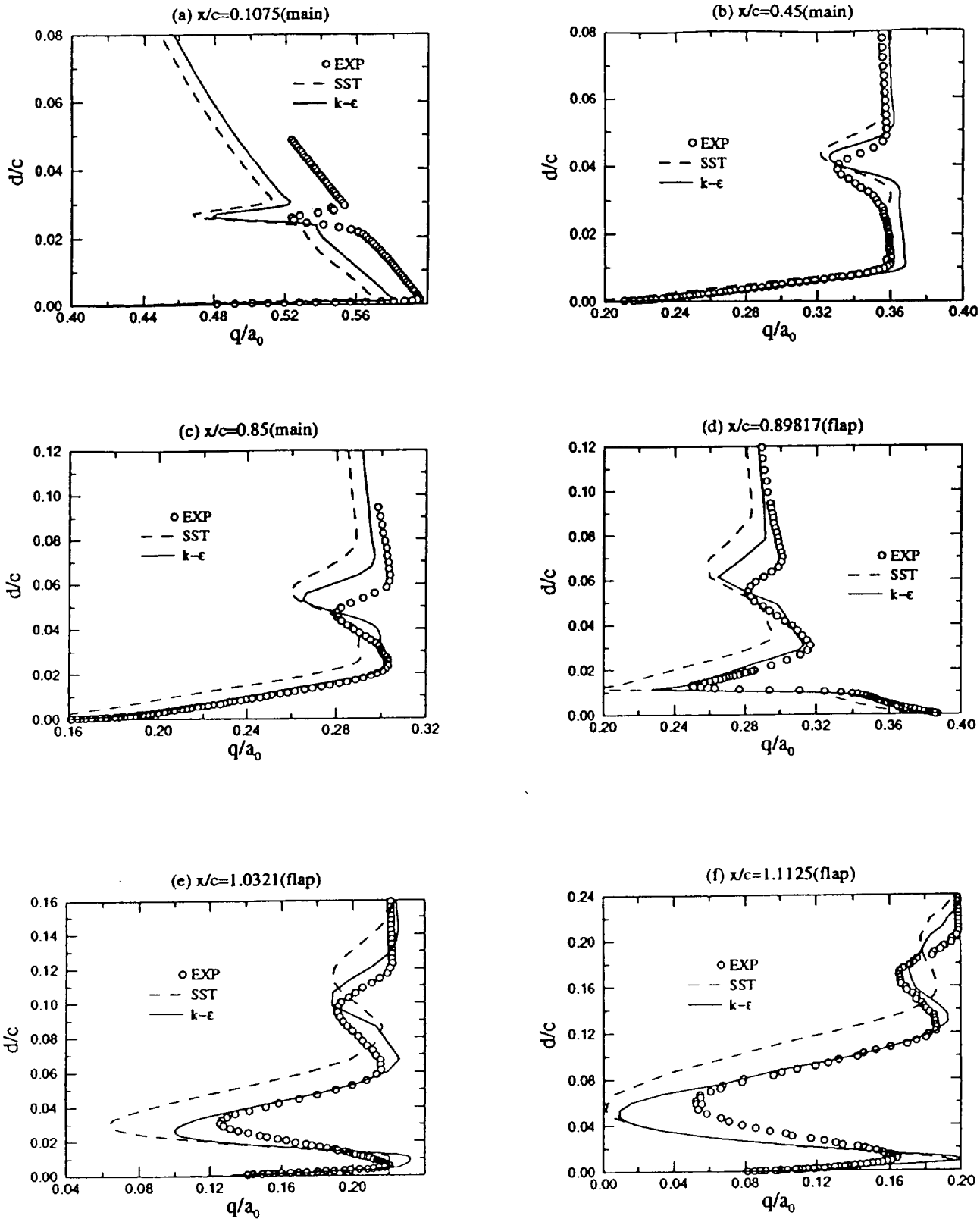

Figure 5. Velocity profiles. 19^0

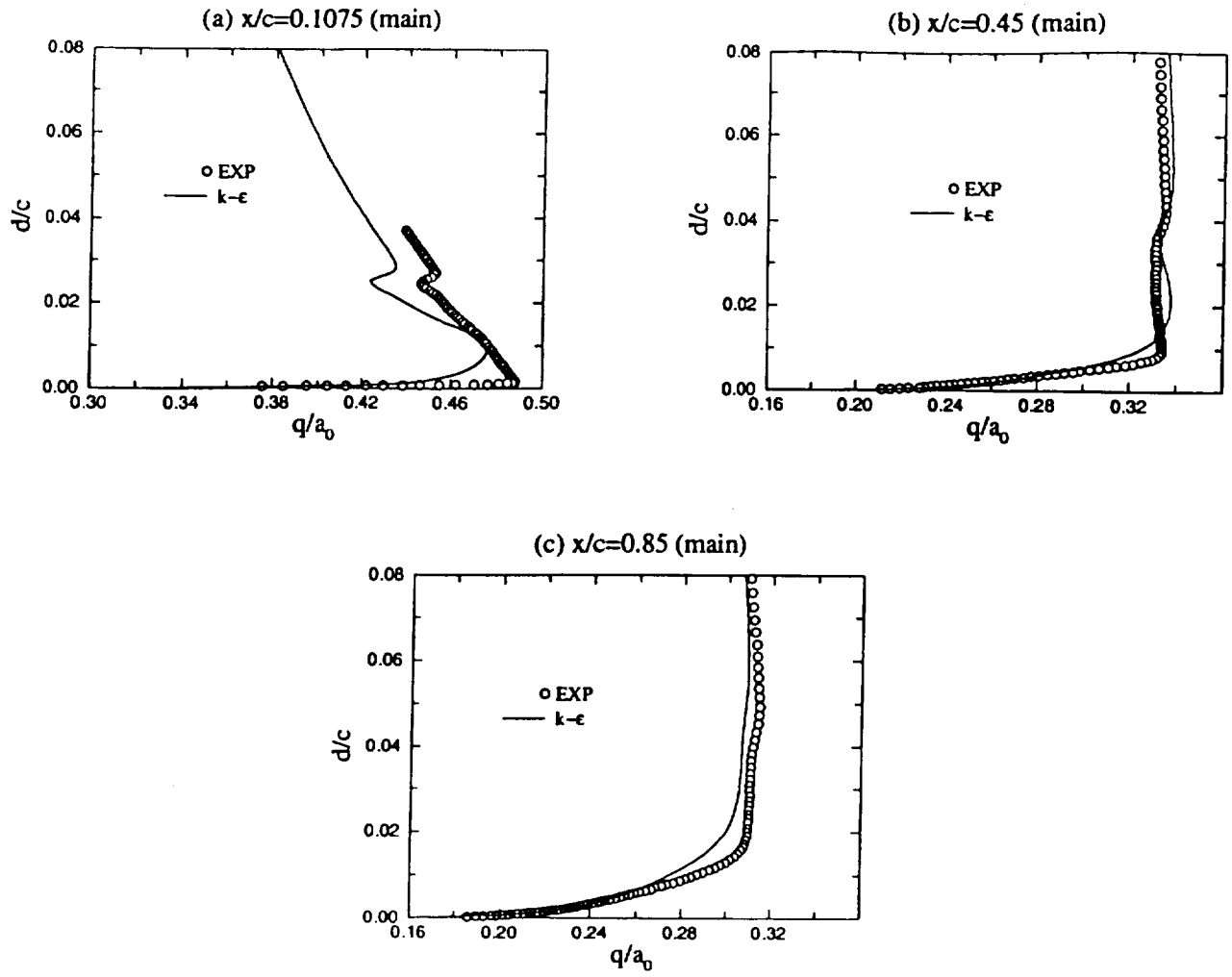

Figure 6. Velocity profiles. 8^0

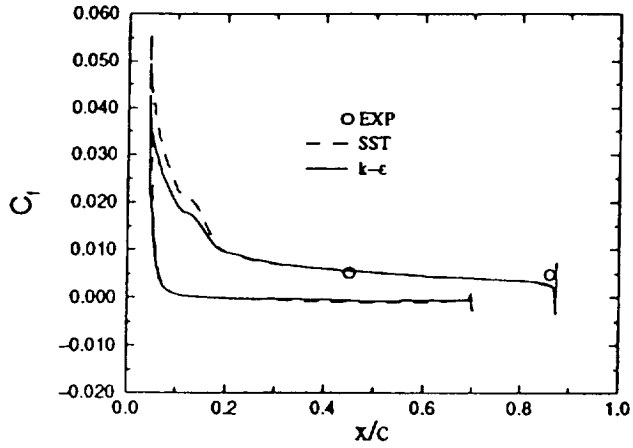

Figure 7. Skin friction coefficient. 19^0

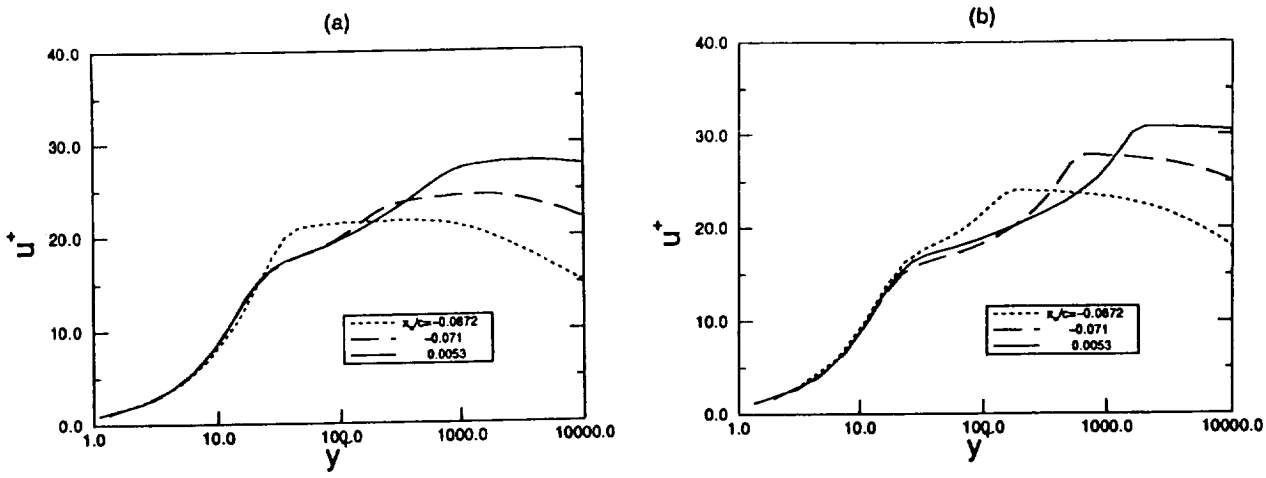

Figure 8. Slat Velocity profiles. (a) 8^0; (b) 19^0.

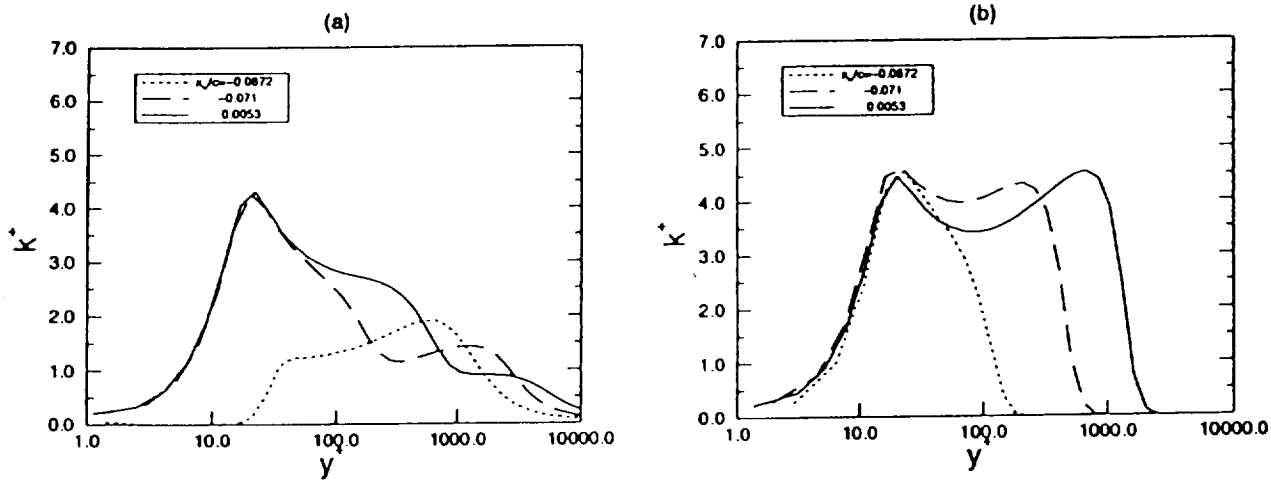

Figure 9. Slat turbulent kinetic energy.(a) 8^0; (b) 19^0.